Three-dimensional fluid simulations of plasma asymmetries in the Martian magnetotail caused by the magnetic anomalies

E. M. Harnett and R. M. Winglee

Department of Earth and Space Sciences, University of Washington, Seattle, Washington, USA

Received 6 November 2003; revised 18 April 2005; accepted 22 April 2005; published 23 July 2005.

[1] Three-dimensional single fluid nonideal MHD simulations of the solar wind interaction with Mars show that the strong magnetic anomalies in the Southern Hemisphere of Mars cause asymmetries in the near tail plasma. The simulations were run with the strong southern magnetic anomalies (SSMA) facing midnight, dawn, or dusk. The interplanetary magnetic field (IMF) was set to 1 nT in the B_y direction. The steady state results were then compared to the case when no surface magnetic field is present. The comparisons show regions of plasma depletion of ~60% and enhanced plasma densities of over 200% for different SSMA orientations. The depleted plasma regions are similar to the plasma voids detected by Mars Global Surveyor. A minimagnetopause forms inside the magnetic pileup boundary for all three cases. When the SSMA are at the dusk terminator, the IMF drapes over dipole-like surface magnetic fields, creating a magnetic field geometry reminiscent of a closed magnetosphere at Earth. When the SSMA are at dawn, the magnetic field geometry resembles that of an open magnetosphere at Earth, as the IMF reconnects substantially to the surface magnetic field. The complex magnetic field geometry for all three cases presented leads to large-scale modification of the plasma flow in the tail.

Citation: Harnett, E. M., and R. M. Winglee (2005), Three-dimensional fluid simulations of plasma asymmetries in the Martian magnetotail caused by the magnetic anomalies, *J. Geophys. Res.*, *110*, A07226, doi:10.1029/2003JA010315.

1. Introduction

[2] Mars Global Surveyor discovered strong magnetic fields of crustal origin at Mars [*Acuna et al.*, 1999; *Connerney et al.*, 1999], with peak magnetic field magnitudes in excess of 1000 nT. These magnetic anomalies are localized primarily in the Southern Hemisphere, within 120° longitude. The magnetic anomalies resembles a "bar code" pattern with the width of the stripes on the order of 100 km, and length on the order of 2000 km. While the Viking and Phobos missions could not definitively prove the existence of a intrinsic magnetic field at Mars, analysis of the data, in conjunction with simulations, suggested Mars possessed a weak intrinsic magnetic field. *Shinagawa and Cravens* [1989, 1992] investigated the role of a weak intrinsic magnetic field on the structure of the ionosphere with a 1D multispecies MHD model. Comparison of the simulation results to the values measured by the Viking landers, indicated that the model that produced the best fit to ion densities as a function of altitude, assumed that both an induced and intrinsic magnetic field were present. The upper limit on the intrinsic magnetic field was 30 nT. However, both Viking 1 and Viking 2 landed in regions in the Northern Hemisphere that MGS data indicates as having no crustal magnetization or being weakly magnetized. The simulations by *Shinagawa and Cravens* [1989, 1992] did suggest though, that an intrinsic magnetic field may locally modify the structure of the ionosphere by a measurable amount.

[3] A similar conclusion was arrived at by *Axford* [1991]. Two results from the Phobos 2 mission led *Axford* [1991] to conclude that a weak, intrinsic magnetic field was modifying the plasma inside the Martian magnetosphere. The first result was the indication that the upward diffusion of plasma was suppressed in the topside ionosphere, consistent with the presence of an intrinsic magnetic field. The second result was the presence of high energy heavy ions. Analyzing Phobos 2 data, *Lundin et al.* [1990] found large O^+ outflows in the tail that were highly variable. They also found regions of locally high O_2^+ outflows. *Axford* [1991] concluded from the energy spectrum and pitch angle distribution that a process like magnetic field reconnection was necessary to generate the high energy ion populations.

[4] While these, results prior to the discovery of the magnetic anomalies by MGS, did not suggest the nature of the intrinsic magnetic field, they did suggest the possibility of local ionospheric and magnetospheric variability. Reanalyzing Phobos 2 data, in light of the MGS discovery of the crustal magnetic fields, *Verigin et al.* [2001] found modulation of the magnetotail thickness by the magnetic anomalies. The magnetotail boundary was defined by the

0148-0227/05/2003JA010315$09.00

location of the magnetic pileup boundary (MPB), with the signature being the disappearance of solar wind protons. When the southern anomalies were at the terminator, they found that the magnetotail increased in width by 500–1000 km.

[5] Previous simulations of the solar wind interacting with a magnetized Mars by *Ma et al.* [2002] and *Harnett and Winglee* [2003] were run with the strongest anomalies on the dayside, facing into the solar wind. The three-dimensional (3-D) MHD simulations by *Ma et al.* [2002] found no large change in the location of the bow shock relative to an unmagnetized Mars. However, the altitude of the ionopause did show variation with surface magnetic field. They also saw asymmetry in the magnetic field in the tail, and the presence of closed magnetic fieldlines, or minimagnetocylinders on the nightside, like those proposed by *Mitchell et al.* [2001].

[6] Three-dimensional nonideal MHD fluid simulations by *Harnett and Winglee* [2003] generated a minimagnetopause in place of an MPB over the strong southern magnetic anomalies (SSMA) near the noon meridian. The simulations also showed the nonideal MHD nature of both the minimagnetopause and the MPB. For the cases shown in *Harnett and Winglee* [2003], the minimagnetopause formed at a higher altitude than the MPB in the Northern Hemisphere. This complimented results from *Crider et al.* [2002]. They looked at the longitudinal and latitudinal distribution of MPB crossings by MGS and found that the MPB is typically 500 km further from the surface in the Southern Hemisphere than in the Northern Hemisphere.

[7] The previous fluid simulations by *Ma et al.* [2002] and *Harnett and Winglee* [2003] looked only at a magnetic field orientation with the strongest magnetic anomalies on the dayside. In addition, results presented in the work of *Harnett and Winglee* [2003] focused on the modification of the plasma by the magnetic anomalies in a region only a few hundred kilometers from the surface. This paper presents 3-D single fluid, nonideal MHD simulation results showing the change in plasma characteristics in the Martian magnetotail when the strongest magnetic anomalies are at locations other than near the noon meridian. The results in this paper show that large-scale structures can form in the tail due to the presence of the magnetic anomalies. The size and scope of the modifications to the tail plasma are compared relative to the case when no magnetic anomalies are present. This paper also discusses how the interaction of the anomalous magnetic field with the IMF varies when changing the planetary orientation, resulting in modification of the location and size of plasma asymmetries both in the tail and near the surface.

2. Model

[8] The simulations solve the following equations using the 2-step Lax method [*Richtyer and Morton*, 1967] in 3-D, on a nested grid system. The resolution of the finest grid is equal to 109 km, and 435 km in the coarsest grid. The coordinates are such that $\vec{z}$ is perpendicular to the ecliptic plane, $\vec{y}$ is in the ecliptic plane but perpendicular to the solar wind velocity, and $\vec{x}$ is in the direction of the solar wind bulk velocity. All of the grids have 75 grid points in the x direction, 105 in the y direction, and 75 in the z direction. The midpoint of all the grids along the z axis is at the equator, and the midpoint of all the grids along the y axis is at the noon meridian. The grids are then situated along the x axis such that the transition between grid systems does not overlap the bow shock or MPB.

[9] The nonideal MHD equations are:

$$\frac{\partial \rho_m}{\partial t} + \nabla \cdot \mathbf{m} = 0 \tag{1}$$

$$\frac{\partial \mathbf{m}}{\partial t} + \nabla \cdot \left(\mathbf{m} \frac{\mathbf{m}}{\rho_m} \right) + \nabla P = \mathbf{J} \times \mathbf{B} + \rho_m \mathbf{g}(\mathbf{r}) \tag{2}$$

$$\frac{\partial e}{\partial t} + \nabla \cdot \left(\frac{\mathbf{m}}{\rho_m} (e + P) \right) = \mathbf{E} \cdot \mathbf{J} + \mathbf{m} \cdot \mathbf{g}(\mathbf{r}) \tag{3}$$

$$\frac{\partial \mathbf{B}}{\partial t} + \nabla \times \mathbf{E} = 0 \tag{4}$$

$$\mathbf{J} = \nabla \times \mathbf{B} \tag{5}$$

$$\mathbf{E} = -\mathbf{v} \times \mathbf{B} + \eta \mathbf{J} + \frac{1}{q n_e} (\mathbf{J} \times \mathbf{B} - \nabla P_e) \tag{6}$$

where ρ_m is the mass density of the ion population, **m** is the bulk momentum, **v** is the bulk velocity and equal to $\mathbf{m}/\rho_m$, e is the energy density, **g(r)** is the gravitational vector, **J** is the current density, **B** is the magnetic field, **E** is the electric field, P_e is the electron pressure (and equal to half the total pressure, P), n_e is the electron number density, q is the electron charge, η is the resistivity. The resistivity (η) is nonzero and equal to 10^3 ohm m only inside the inner boundary and the Hall and ∇P_e terms are only evaluated outside the inner boundary.

[10] The inner boundary corresponds to an altitude of 300 km from the surface. At and inside the inner boundary, the density and pressure are held constant to the surface values, with zero momentum. At one grid point above the inner boundary all values are allowed to vary as determined by the above equations. The time dependent magnetic field, associated with the IMF and induced magnetic fields, is allowed to vary in time throughout the interior of the inner boundary. This prevents unphysical pile-up of the IMF at the inner boundary. The value of η is chosen such that unphysical pile-up of the IMF does not occur, but is also at the low end of the range of resistivities for the Martian surface given by *Tang et al.* [1977]. The majority of the IMF will pileup and slip around the planet at the MPB, and/or near the inner boundary as demonstrated by fieldline mapping shown in the next section. The anomalous magnetic field is static in time both inside and outside of the inner boundary and cannot diffuse.

[11] Outside of the inner boundary, numerical diffusion is negligible, and so is omitted from equation (5). Consequently, only the magnetic field components associated with the IMF and its perturbations undergo diffusion inside the inner boundary, as implied by equations (4)–(6). The

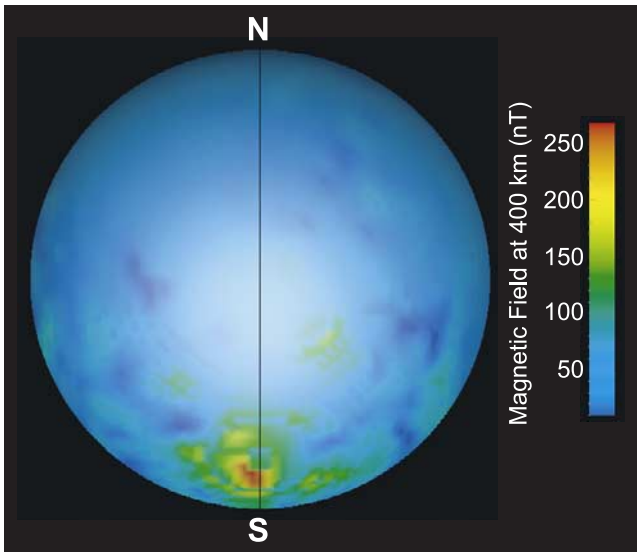

Figure 1. The simulated Martian magnetic field at 400 km from the surface. Owing to lighting and shading that gives the sphere a 3-D appearance, the colors on the spherical surface in this figure and in subsequent figures will not correspond exactly to those shown in the color bar at all locations of the sphere. For the simulations, the anomalous region indicated by the black line (and equivalent to 180°E longitude) was oriented with the dawn or dusk terminator, or at the midnight meridian. In the results presented, the equatorial plane is aligned with the ecliptic plane. From the model provided by *Cain et al.* [2003].

numerical Reynolds number in the simulation grid is on average, about 500, with a larger value near the inner boundary and a slightly smaller value in the solar wind. This implies that reconnection near the inner boundary will be driven solely by the Hall and pressure gradient terms in equation (6), and not by a numerical resistivity.

[12] The solar wind density is equal to 4 ions cm^{-3}, with a bulk speed of 400 km s^{-1}; thus the velocity vector in the defined coordinate system is [400,0,0] km s^{-1}. The Parker spiral approximation of the direction of the IMF at Mars' orbit puts the magnitude of the B_y component 1.5 times larger than the B_x component. Various measurements of solar wind parameters by Phobos 2 and MGS show the magnitude of the IMF in the range of 2–3 nT with the direction in the ecliptic plane primarily in the B_y direction [cf. *Kallio et al.*, 1995; *Vignes et al.*, 2000]. In the results shown below, we will use only the dominant direction. The IMF is only in the $+B_y$ direction with magnitude equal to 1 nT (i.e., the vector for the IMF is [0,1,0] nT).

[13] Viking 1 measured O_2^+ to be the predominant ion species below 300 km. The density at 300 km was approximately 200 cm^{-3}, while the maximum O_2^+ density of 10^5 cm^{-3} occurred at 130 km from the surface [*Hanson et al.*, 1977]. The number density at the inner boundary is set equal to 100 O_2^+ cm^{-3}, with a plasma temperature of 3000 K. These values are held constant throughout the simulation, thus creating both and effective source and sink at the surface. As this is a single fluid simulation, one O_2^+ ion is treated as 32 H^+ ions in setting the mass density at the inner boundary. Increasing the density and temperature beyond these values can lead to strong outflows from the planet that will produce an inflated magnetosphere.

[14] With no solar UV flux, the night side ionospheric density should be greatly reduced. To approximate this, the night side ionospheric density, and thus the pressure, were reduced by an order of magnitude on the night side, with the number density at the nightside inner boundary set to 10 cm^{-3}. The ion density variations associated with solar zenith angle are not included in the model. The decrease in density associated with this effect would be about a factor of two. This is not be as large as the variations in the day-night asymmetry that we use to test how the formation and structure of resulting minimagnetospheres depends on the surface density. Charge exchange and impact ionization processes that lead to planetary neutral ionization by solar wind sources primarily occurs at the MPB [*Riedler et al.*, 1989; *Lundin et al.*, 1989; *Rosenbauer et al.*, 1989; *Vignes et al.*, 2000; *Crider et al.*, 2000]. Asymmetries in the ionospheric density may develop in and around the magnetized regions at the inner boundary, due to increased access of the solar wind to the surface through reconnection of the anomalous magnetic field to the IMF, but predicted asymmetries would need to be calculated from within the model. These asymmetries are not calculated inside the model at this time.

[15] The model of the Martian magnetic field was provided by *Cain et al.* [2003]. A 90 term internal potential function was generated using 110,000 3-component observations from MGS. A map of the magnitude of the magnetic field at an altitude of 400 km (and 100 km above the inner boundary) is shown in Figure 1. For the results presented, the equatorial plane of Mars is aligned with the ecliptic plane. The simulations were run to steady state conditions for a given orientation of the intrinsic magnetic field. The surface magnetic field was only rotated between simulation runs. The SSMA were located at the midnight meridian, and the dawn and dusk terminators.

3. Results

[16] The magnetic anomalies lead to large-scale asymmetries in the tail plasma that change as the orientation of the planetary magnetic field is changed. These asymmetries are present under steady state conditions. For the different orientations of the magnetic anomalies studied, the plasma density, pressure, and temperature are compared to the results when no magnetic anomalies are present on the planet. The case with no magnetic anomalies is used as a baseline for comparison because the model will produce magnetospheric features, such as the tail, that are symmetric about the axis of the solar wind bulk flow. Any asymmetries will be due to the presence of the magnetic anomalies interacting with the plasma.

[17] The size of the asymmetries ranges from a fraction of a Martian radii to more than a Martian radii. In addition, the modification of the plasma is not limited to within a few hundred kilometers of the magnetic anomalies. Instead, asymmetries in the plasma are seen more than two Martian radii from the nightside surface. Asymmetric structures such as tail rays and ionospheric holes have been measured in the wake of Venus [cf. *Dubinin et al.*, 1991; *Brace and Kliore*,

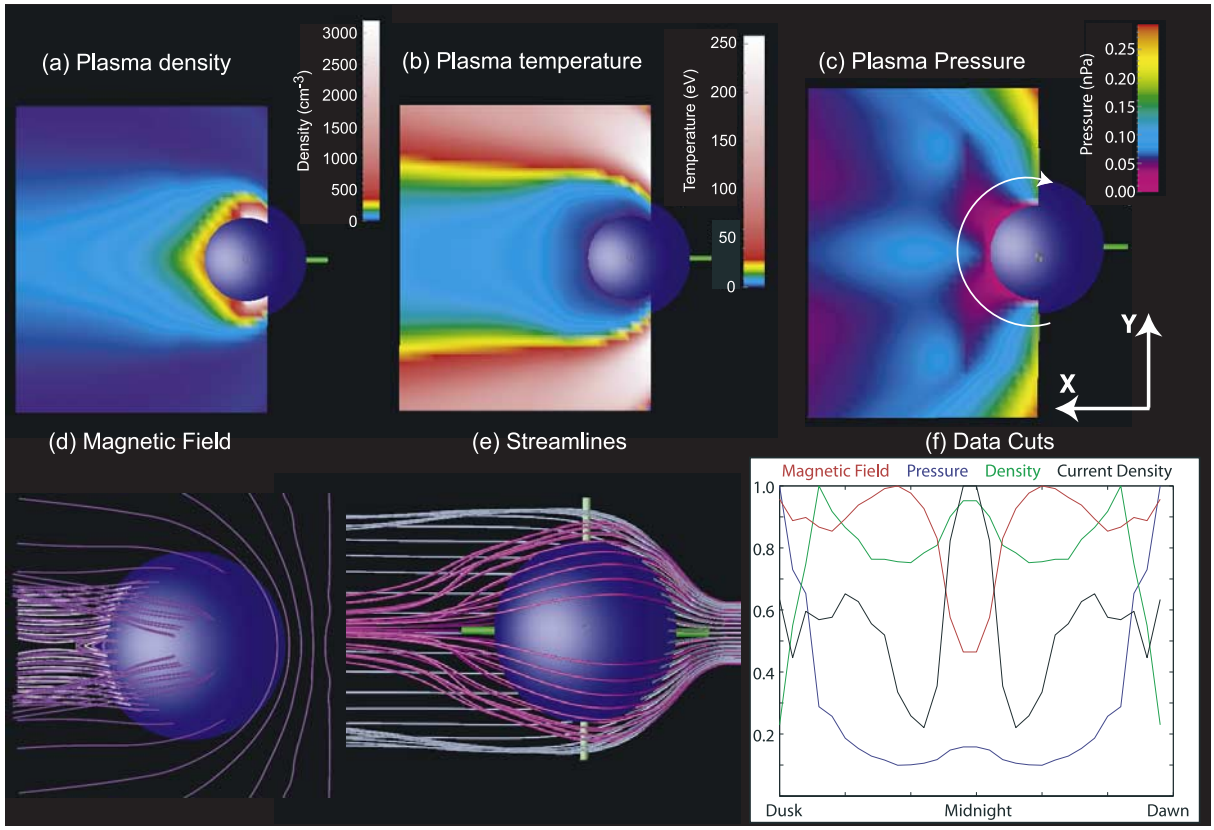

Figure 2. No magnetic anomalies: The (a) density, (b) temperature, (c) pressure, (d) magnetic fieldlines, (e) plasma streamlines, and (f) constant latitude cuts at the approximate location indicated by the white semicircle in Figure 2c. The planes show an area 19,200 by 15,700 km inside the bow shock and are parallel to the equatorial plane but intersect the inner boundary at a latitude of approximately 45°S. The cuts in Figure 2f are taken in the same plane, at a radius of approximately 1300 km above the planet surface, beginning just sunward of the dusk terminator. The different colors of the fieldlines are solely for clarity and do not represent anything physical. The color of the streamlines merely differentiates between streamlines originating from two different dayside locations. The sampled values in Figure 2f are shown in normalized units. The normalizing factor for the magnetic field magnitude is equal to 9.3 nT, 0.403 nPa for the pressure, 4.12 nA (m^{-2}) for the current density, and 185 cm^{-3} for the effective number density.

1991]. These simulation results suggest that the magnetic anomalies will cause asymmetries in addition to those that would form when the solar wind can interact with the planetary ionosphere, as found at an unmagnetized planet.

3.1. No Crustal Magnetic Field

[18] Figure 2 shows the density, temperature, pressure, magnetic field configuration, and plasma streamlines in the tail region when no anomalies are present. Here the tail is defined as the entire region inside the magnetosheath, where the boundary between the two regions is the transition from plasma with a temperature on the order of 200 eV to a region where the plasma temperature is on the order of 10 eV. The density (Figure 2a) shows the effective number density. As this is a single fluid model, the number density of 100 O_2^+ ions cm^{-3} at the dayside inner boundary has an effective number density of 3200 cm^{-3}. The density, temperature and pressure are shown in a plane parallel to the equatorial plane, but intersecting the inner boundary at approximately 45°S. Images Figures 2a–2e are viewed from above the south pole. The area shown is inside the bow shock. The hot plasma in the flanks is magnetosheath plasma. Also shown is the total magnetic field configuration (Figure 2d) and the streamlines for the plasma flow (Figure 2e). The magnetic fieldline density is not a true representation of the magnitude of the magnetic field, but instead gives a representative picture of the geometry. The color of the magnetic fieldlines is solely for clarity. The color of the streamlines denotes streamlines originating from two different locations upstream. The magnetic field can be seen draping around the planet on the dayside and sliding over the poles. The closed magnetic fieldlines near the midnight meridian are due to IMF that has diffused through the planet. The streamlines show the flow originating on the dayside, diverting around the planet and then out the tail.

[19] Figure 2f shows a sampling of the simulation density, pressure, current density, and magnetic field magnitude in the planes in Figures 2a–2c, at a radius of approximately 1300 km. The white curve in Figure 2c indicates the direction and approximate location that the simulation results were sampled. From these cuts, we can further see the symmetry of the results for an unmagnetized planet.

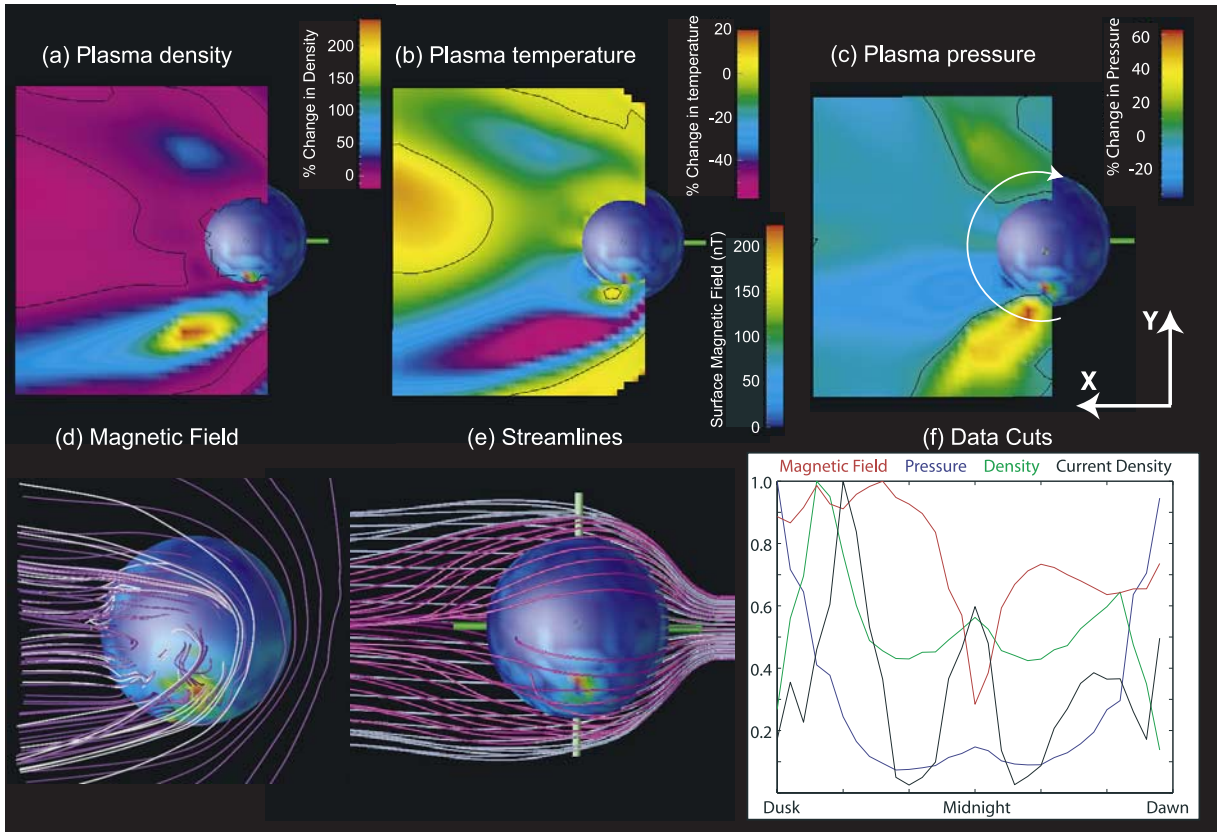

Figure 3. SSMA at the dusk terminator: The percent change in (a) density, (b) temperature, and (c) pressure relative to when no anomalies are present. (d) Magnetic fieldlines are shown along with (e) streamlines. The origin of the streamlines is identical to that in Figure 2. (f) The values sampled are at the same location as in Figure 2. The horizontal planes are the same size and at the same location as in Figure 2. The black contours in Figures 3a, 3b, and 3c indicate a value of zero percent change. The sampled values in Figure 3f are absolute values, not percent change, with the normalizing factors equal to 12.2 nT for the magnetic field magnitude, 0.439 nPa for the pressure, 9.77 nA m^{-2} for the current density, and 337 cm^{-3} for the effective number density.

They also show the structure of the tail plasma near the planet. The density at the center of the tail is comparable to the density at the terminator, where the effects of the elevated dayside surface density can be seen. At the center of the tail, the magnetic field magnitude is minimal, while the current density is at maximum.

3.2. SSMA at Dusk

[20] Figures 3a–3c show the percent change in the density, temperature and pressure with respect to when no anomalies are present, for the SSMA at the dusk terminator. The magnitude of the anomalous magnetic field at 300 km is mapped onto a sphere representing the inner boundary. The view angles and areas shown are the same as in Figure 2. The percent change is calculated at each grid point using the formula

$$\text{percent change} = \frac{(\text{with anomaly}) - (\text{no anomaly})}{\text{no anomaly}} \times 100 \quad (7)$$

The black contour lines in Figures 3a–3c (and all subsequent percent change plots) indicates a value of zero percent change. The origin of the streamlines is identical to those in Figure 2e. The sampled simulation results in Figure 3f are taken from the same locations as in Figure 2f and show the actual values, not the percent change.

[21] For this configuration, the plasma density more than doubles and the pressure increases by 50% (Figures 3a and 3c) in the dusk side flank, while the temperature decreases in the same region (Figure 3b). This is the largest change in plasma density for the three orientations of the SSMA shown. Near the inner boundary, all three quantities, pressure, density and temperature show a positive percent increase. The density enhancement can also be seen in the sampled data (Figure 3f).

[22] The magnetic field (Figure 3d) and plasma bulk flow (Figure 3e) indicate two processes are occurring in the tail. The pileup of the IMF is enhanced as it is predominately in the same direction as the non-B_z portion of the planetary and induced magnetic field (i.e., the combination of both the anomalous magnetic field and the magnetic field generated by the current systems near the SSMA). Directly above the strongest surface magnetic fields,a rounded, dipole-like magnetic field forms (Figure 4). At altitudes above those magnetic field loops, the IMF, that is sliding over the south pole (white fieldlines in Figure 3d), drapes over this dipole-

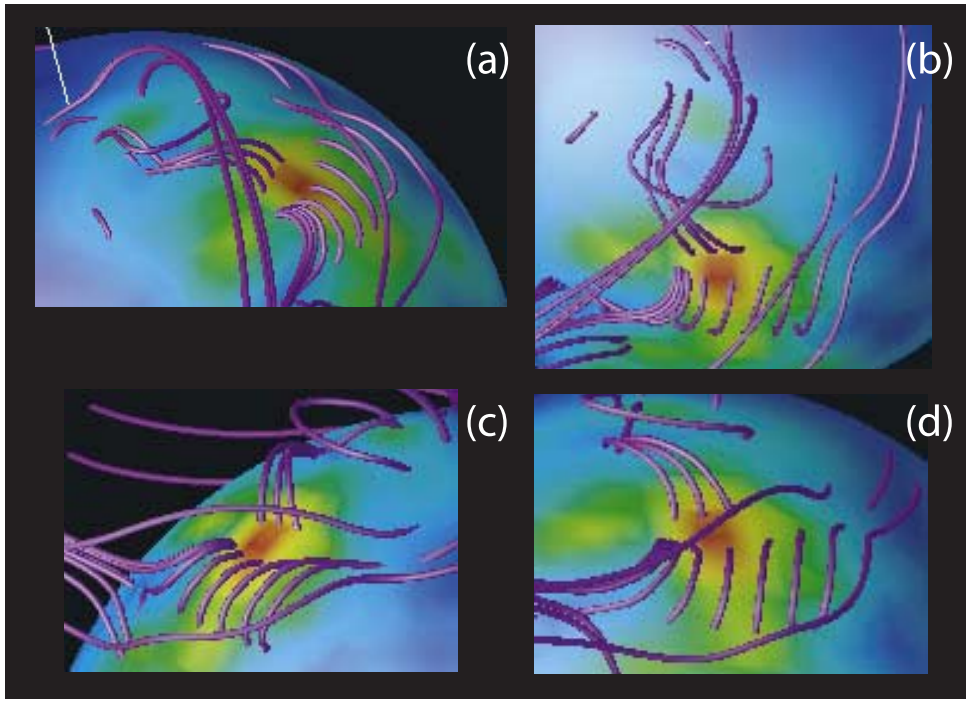

Figure 4. The magnetic field configuration when the SSMA are on the dusk side for four different look directions. The magnetic fieldlines shown are the same in all four figures but as a subset of those shown in Figure 3. Only the area around the SSMA region is shown. Figure 3b is from the same look direction as Figure 3d, while Figure 3a is viewed from the tail, with the axis of the south pole visible in the upper left corner. Figure 3c is viewed from the dayside, near the equatorial plane, and Figure 3d is viewed from dusk terminator near the equator.

like magnetic field (Figures 3d and 4). This leads to a quasi-closed minimagnetosphere configuration. This can also be seen in the cuts of the magnetic field magnitude (Figure 3f). An extended region of enhanced magnetic field magnitude forms near the SSMA. As a result, the plasma streaming around the side of the planet is pushed further from the surface, widening the tail. This can be seen in comparing the purple streamlines in Figures 2e and 3e. Both sets of streamlines originate from the same location on the day side, but in the dusk configuration those streamlines spread out in the tail, in comparison to when no magnetic anomalies are present. Broadening of the tail will lead to elevated densities and reduced temperatures in the flank regions relative to when no anomalies are present. Excluding the region near the inner boundary, the highest densities and lowest temperatures are near the core of the tail. Thus broadening of the tail causes enhancement of the density relative to when no anomalies are present.

[23] The second process leading to the enhanced region on the dusk side occurs much closer to the inner boundary, and is due to the formation of a minimagnetopause. Previous simulations by *Harnett and Winglee* [2003] showed that when the SSMA are on the dayside, a minimagnetopause formed in place of the MPB. At the MPB, the thermal pressure gradient was small and the magnetic field was consistent with draping of the IMF. Also the thickness of the current layer indicating the location of the MPB was at most 300 km. In contrast, there was a large gradient in the thermal pressure at the minimagnetopause. The current region associated with the minimagnetopause was also substantially larger both in physical size, at 600–1200 km thick, and in magnitude of the peak current density. Those simulations found that the best parameters for distinguishing between a minimagnetopause and the MPB are pressure and the magnitude of the current. This remains true when the SSMA are not on the dayside and is what will be used to determine the nature of the enhanced regions seen in the results and presented in this paper.

[24] When the SSMA are on the dusk side, a region of large current density forms inside, and separate from, the MPB. Figure 5 shows the magnitude of the current density in a plane running parallel to the terminator and intersecting the surface 500 km to the day side of the strongest anomalous magnetic field. The outer most current layer encircling the planet is the MPB. The current region inside the MPB on the dusk side is a minimagnetopause. This region of enhanced current density can also be seen in the sampled current density in Figure 3f. Both the temperature and the pressure are elevated in this region, further supporting that a minimagnetopause forms inside the MPB. The beginning and ends of the traces in Figure 3f sample two grid points to the day side of the terminator to capture most of the affected region. Owing to the large pressures on the day side of the magnetosphere, the pressure enhancement associated with the minimagnetopause appears as a softening of the slope of the pressure trace on the dusk side as compared to when no magnetic anomalies are present. The enhanced temperature region forms in a magnetosheath-like region.

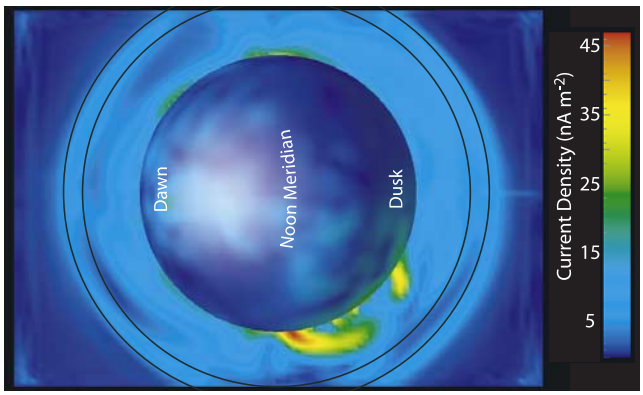

Figure 5. The magnitude of the current density in a plane parallel to the terminator when the SSMA are on the dusk side. The plane intersects the planet 500 km toward the day side of the strongest anomalous magnetic field and is 14,900 by 10,700 km. The black lines indicate the inner and outer edge of the MPB for the case with an unmagnetized Mars.

[25] The quasi-closed magnetic field geometry means that plasma flow to the surface is inhibited. This pushes the MPB out from the surface. The dotted black lines in Figure 5 indicate the inner and outer edges of the MPB when no magnetic anomalies are present. The outer edge was defined as the location where the current density becomes greater than 1–2 nA m^{-2}. The interior line marks the inner edge of the shell where current density exceeds 10 nA m^{-2}. Further inside this region defined as the MPB, the current density reduces to 5 nA m^{-2} before increasing again near the surface. The MPB just opposite the anomalous region forms approximately 330 km (or 3 grid points) further from the surface than when no anomalies are present. This is comparable to the value of 500 km that *Crider et al.* [2002] determined to be the average increase in MPB altitude in the Southern Hemisphere.

3.3. SSMA at Dawn

[26] When the SSMA are on the dawn side (Figure 6), the currents are such that the IMF reconnects to the crustal magnetic field over a significant portion of the anomalous region. This is different from the dusk SSMA case, where the IMF sliding over the south pole primarily drapes over the top of the magnetic anomalies. This reconnection of the IMF with the non-B_z portion of the planetary and induced

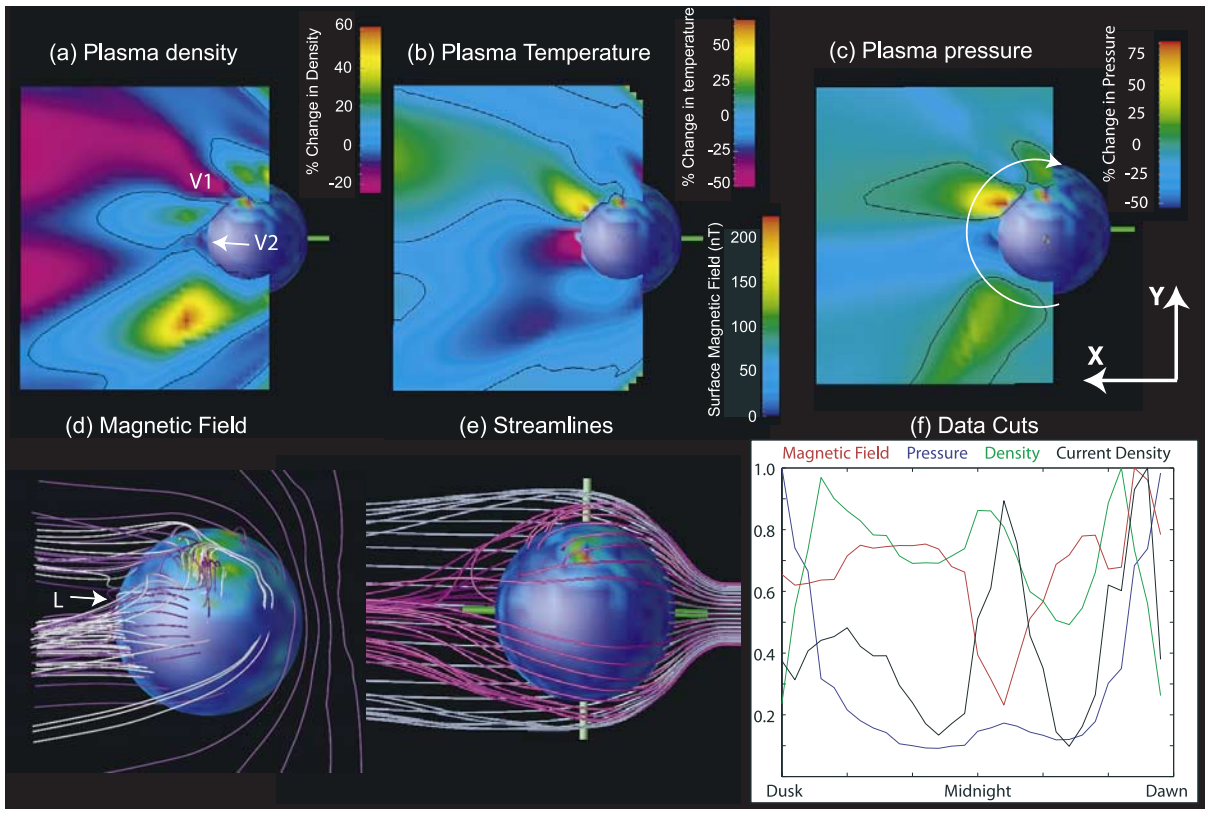

Figure 6. SSMA at the dawn terminator: The percent change in (a) density, (b) temperature, and (c) pressure relative to when no anomalies are present. (d) Magnetic fieldlines are shown along with (e) streamlines. The origin of the streamlines is identical to that in Figure 2. (f) The values sampled are at the same location as in Figure 2. The horizontal planes are the same size and at the same location as in Figure 2. The normalizing factors for the sampled values in Figure 2f are equal to 13.1 nT for the magnetic field magnitude, 0.384 nPa for the pressure, 7.66 nA m^{-2} for the current density, and 232 cm^{-3} for the effective number density.

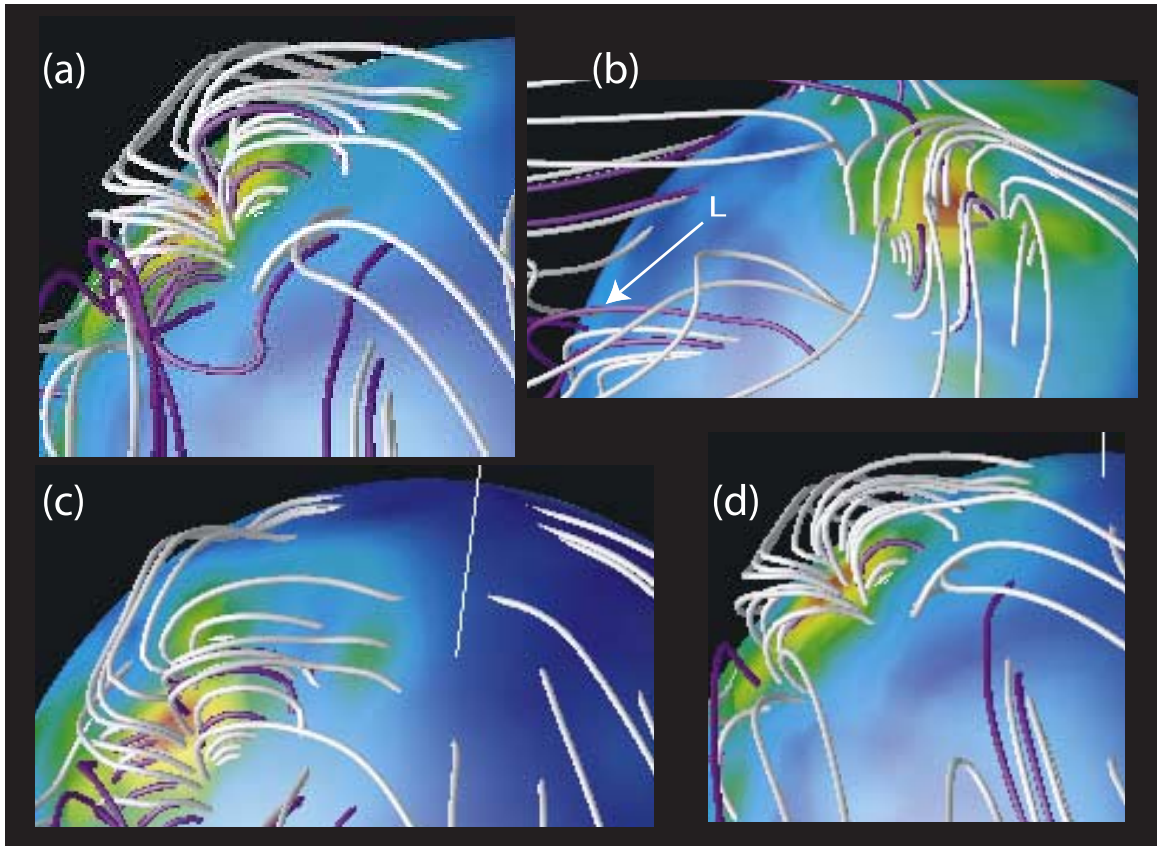

Figure 7. The magnetic field configuration when the SSMA are on the dawn side for four different look directions. The white fieldlines are the same in all four figures, while the number of purple fieldlines shown varies. All the magnetic fieldlines shown are a subset of those shown in Figure 6. Figure 7b is from the same look direction as Figure 6d for only the region around the SSMA. Figures 7a and 7d are viewed from the tail, with the south pole in the upper right corner. Figure 7c is viewed from the tail near the south pole. The line indicating the polar axis appears in the middle of the figure.

magnetic field creates a cusp-like structure on the midnight side of the large anomalous region (Figures 6d and 7), This can be seen in the white magnetic fieldlines of IMF origin, that drape around the dayside of the south pole. On the dusk side these fieldlines are swept into the nightside and do not connect to the planet. However, on the dawn side, these fieldlines connect to the surface magnetic field. This leads to increased access to the surface, and a quasi-open mini-magnetosphere. Associated with this magnetic field geometry is a flow of plasma toward the surface (Figure 6e), which can be seen in the pink streamlines impacting the surface near the anomalous region. It can also been seen in the sampled magnetic field magnitude in Figure 6f. At one sampled location on the dawn side, the magnetic field magnitude is comparable to the maximum value for the dusk configurations. However the strength of the magnetic field in the extended region around the anomaly is comparable only to the maximum value for the case with no magnetic anomalies. This indicates a reduced total magnetic field strength due to a process like reconnection.

[27] This magnetic field configuration leads to a void region (V1) forming downstream of the anomalies as the plasma flowing around the planet is directed toward the surface instead of continuing down the tail (Figures 6a and 6e). Another void region (V2) forms in the midnight sector that corresponds with the gap in the magnetic fieldlines. In between these two void regions, on the dawn side of the midnight meridian, there is a region where the temperature and the pressure of the plasma are respectively 30% and 75% larger than when no anomalies are present. This coincides with closed magnetic fieldlines running longitudinally along the surface (L in Figures 6d and 7). Plasma is deflected toward the surface in this region but the closed magnetic fieldlines running along the surface prevent access. This leads to the formation of a structure similar to a minimagnetopause, with enhancements in density, temperature and pressure. The enhancement in the density and decrease in the temperature on the dusk side is due to broadening of the tail by smaller anomalous regions on the dusk side.

[28] The current (Figure 8) indicates that a minimagnetopause still forms around the SSMA inside the MPB when the SSMA are on the dawnside (and can also be seen in the current density in Figure 6f). However, the MPB is in approximately the same location as when no anomalies are present due to the decrease in total magnetic field magnitude. This reduction in magnetic field magnitude is due to an increase in reconnection of the IMF to the anomalous magnetic field, and the formation of a cusp-like magnetic field configuration. Thus the total magnetic field

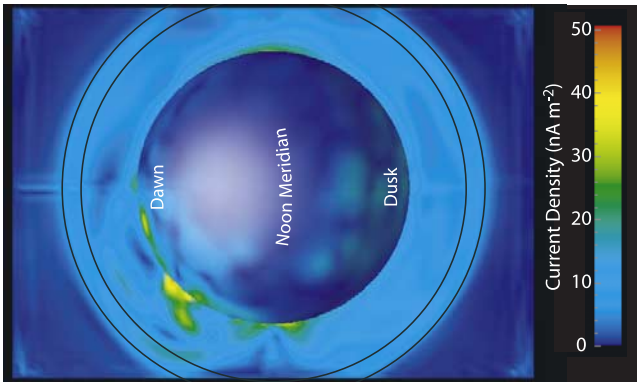

Figure 8. The magnitude of the current density in a plane parallel to the terminator when the SSMA are on the dawn side. The plane is at the same location as in Figure 5. The black lines indicate the inner and outer edge of the MPB for the case with an unmagnetized Mars.

determines if the MPB is pushed out. The pressure at the minimagnetopause is also reduced from the pressure enhancement at the minimagnetopause when the SSMA are on the dusk side, due to the increased access to the surface. The density in the minimagnetopause region is also not as large as for the dusk configuration (Figure 6f). Therefore, while a minimagnetopause forms in both dusk and dawn SSMA orientations, the effect that it will have on the entire magnetosphere will be highly dependent on the total magnetic field geometry. The characteristics seen for the dusk SSMA orientation cannot be generalized to make predictions about the dawn orientation, even though a minimagnetopause forms in both cases.

3.4. SSMA at Midnight

[29] The bulk velocity of the plasma close to the inner boundary for an unmagnetized Mars is around the terminator and toward the surface at the midnight meridian. At distances greater than approximately 1000 km from the surface (at the midnight meridian, in the equatorial plane), the bulk flow switches direction to down the tail. When the SSMA are at midnight (Figure 9), the anomalous magnetic field can prevent plasma from flowing toward the surface, leading to pockets of depleted plasma. The plasma that is deflected away from the surface can then build up in adjacent regions. This leads to enhanced density and pressure in the nearby flank regions.

[30] Moving the SSMA to midnight results in a helical pattern in the magnetic field on the night side (Figures 9c

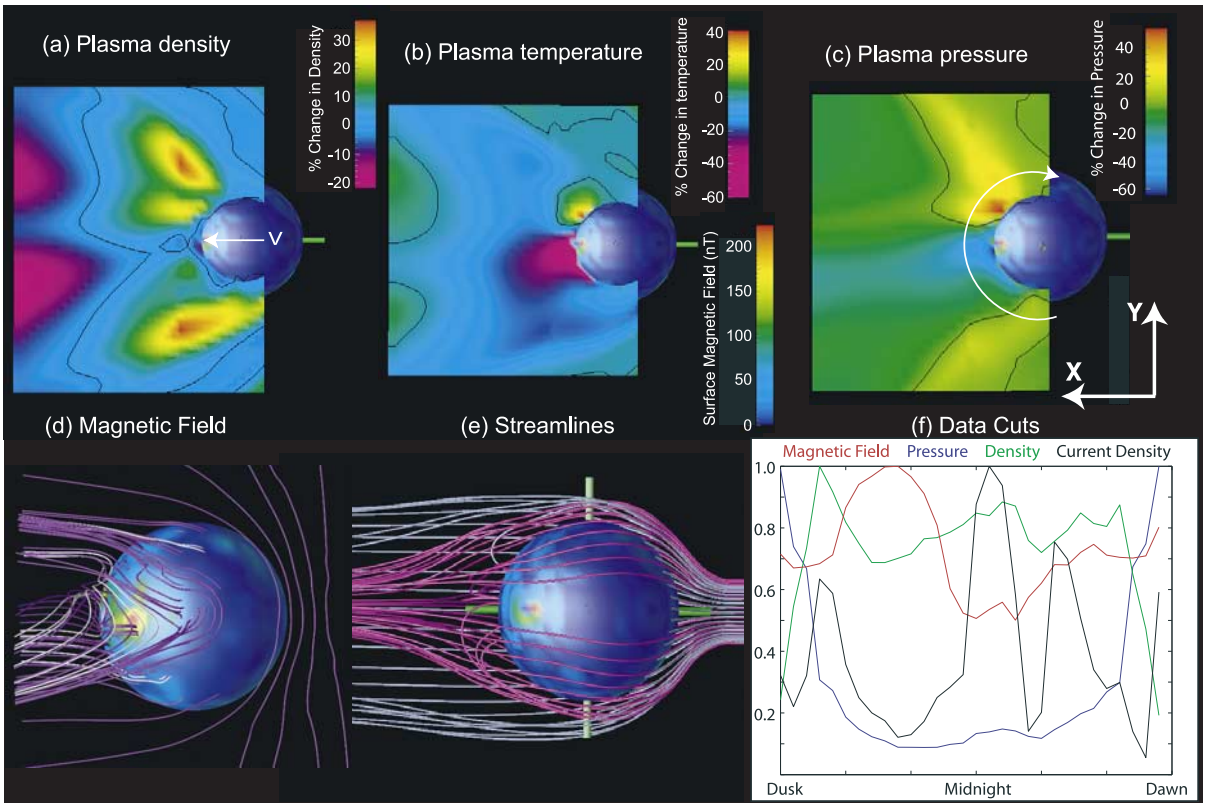

Figure 9. SSMA at midnight: The percent change in (a) density, (b) temperature, and (c) pressure for the strong magnetic anomalies relative to when no anomalies are present. (d) Magnetic fieldlines are shown along with (e) the streamlines. The origin of the streamlines is identical to that in Figure 2. (f) The values sampled are at the same location as in Figure 2. The horizontal planes for density and pressure are the same size as in Figure 2, while the change in the temperature is shown in a plane 17,000 by 15,700 km. All planes at the same location as in Figure 2. The normalizing factors of the sampled values in Figure 9f are equal to 12.4 nT for the magnetic field magnitude, 0.397 nPa for the pressure, 7.58 nA m^{-2} for the current density, and 219 cm^{-3} for the effective number density.

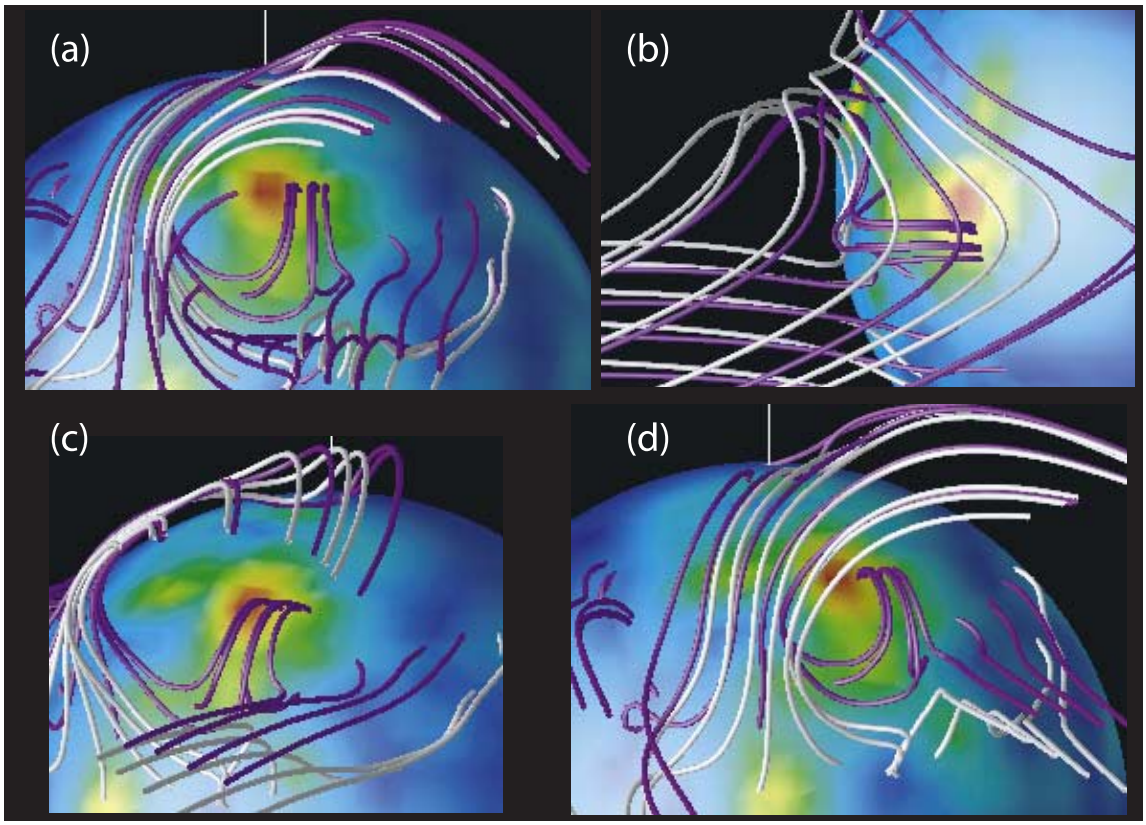

Figure 10. The magnetic field configuration when the SSMA are at midnight for four different look directions. The magnetic fieldlines shown are the same in all four figures but as a subset of those shown in Figure 9. Figure 10b is from the same look direction as Figure 9d with only the area around the SSMA region shown. Figure 10a is viewed from the tail, near midnight in the equatorial plane. Figure 10c is viewed from the dusk sector, and Figure 10d from the dawn sector, both also along the equatorial plane.

and 10). The helical shape of the magnetic field blocks plasma from the dawnward and southern side of the planet from flowing into the region near the SSMA, and the density is enhanced in this region (Figures 9a and 9f). The enhanced temperature (Figure 9b) in the region suggests that a minimagnetopause boundary forms, as opposed to a stagnation point. A stagnation point will have an enhanced density and pressure, but the temperature will not be enhanced. The fact that the current density is large in this region, in conjunction with the enhancements in the pressure, density and temperature, indicates the formation of a minimagnetopause. The enhancement in the current density can be seen in Figure 9f. On the dusk side of the midnight meridian, the direction of the magnetic field is such that the helix allows for partial plasma entry and thus only diverts the plasma flow. As a result, the plasma density is only slightly enhanced in this region and a minimagnetopause does not form on this side. The density enhancements in the flanks are again due to broadening of the tail in that region, relative to when no anomalies are present.

[31] The streamlines (Figure 9e) indicate substantial plasma flow toward the surface in the midnight sector, near the equator. This corresponds to the northern edge of the helical magnetic field pattern, where the magnetic field connects to the planet, forming an extended cusp-like region. The net result for the SSMA on the night side though is large-scale diversion, creating the plasma void in the midnight sector around the SSMA (V in Figure 9a).

3.5. Comparison of SSMA Cases

[32] The results for three different orientations of the crustal magnetic field show that few generalizations can be made regarding the structure of the resulting minimagnetospheres around the anomalous magnetic field. For each SSMA orientation, a minimagnetopause formed, but each minimagnetopause has its own unique structure. This leads to differences in the effect of a minimagnetopause on the large-scale plasma structures in the entire tail, such as the location of the MPB.

[33] The formation of cusp-like structures due to reconnection of the anomalous magnetic field to the IMF, changes the plasma flow toward the surface with respect to an unmagnetized Mars. Streamlines impacting the inner boundary (Figures 3e, 6e, and 9e), also suggest increased plasma flow toward the surface. However, the flaring of the streamlines in the down tail region indicates that the increase in flow toward the surface in some regions may be tempered by a decrease in flux toward the surface in other regions. To estimate the change in flux, the direction and magnitude of the radial component of the momentum was summed over a spherical surface 1000 km from the surface and 700 km from the simulation boundary at the planet, for each magnetic field configuration. When com-

pared to the value for the case with no surface magnetic field, these sums suggest that the flux of plasma toward the surface is larger when the SSMA are in the dawn and midnight sectors, and smaller when they are on the dusk side. A better measurement of the flux will come in the future with expansion of the code to multifluid so that solar wind and ionospheric populations can be tracked separately.

[34] *Verigin et al.* [2001] found that the width of the magnetotail was modulated by the location of the strongest magnetic anomalies, as measured at approximately $3R_M$ by Phobos2. In the simulations, the strong current signature seen at the MPB, near the planet, diminishes in the tail. Therefore it is much harder to quantitatively determine the MPB location, and thus the boundary for the magnetotail. The increase in density and temperature as measured by the percent change shown above indicated that near the planet, the tail broadens, although asymmetrically, for all three configurations. When the tail width is measured using the transitions from hot sheath plasma to cooler tail plasma as the boundary layer, only the dusk configuration produces widening of the tail at 11,000 km (3.3 R_M) downstream. The dawn and midnight configurations lead to a narrowing of the tail. This effect can also be seen in Figures 3a, 6a, and 9a. In the tail, near the back of the simulation box, only the dusk SSMA case shows a positive percent change. The dawn and midnight SSMA cases show negative percent changes. As the density increases toward the center of the tail, a positive percent change indicates a flaring of the tail width, and a negative percent change means the tail is narrower. Thus the simulations show that widening or narrowing of the magnetotail not only depends on the location of the anomalies, but also where the tail width is measured.

3.6. Inner Boundary Conditions

[35] To investigate how much the structure of the mini-magnetospheres depends on the nightside density, the density and pressure at the nightside inner boundary were varied. Changes in the ratio of nightside to dayside surface density do not change the overall structure of the plasma asymmetries in the tail, but instead only effect the magnitude of the pressure, density and temperature in the asymmetric regions.

[36] If the nightside surface density is set equal to the dayside surface density, the regions of reduced and enhanced plasma seen in Figures 3, 6, and 9, are present for all three magnetic field orientations. They are just more prominent when the nightside density is reduced. The maximum percent change in the pressure is up to 5 times larger when the nightside density is $\frac{1}{10}$th the dayside density, while the maximum percent change in the density is 3–4 times larger. Decreasing the nightside density and pressure further to $\frac{1}{50}$th of the dayside density only leads to small increases in the magnitude of the percent change in density and pressure though.

[37] A reduced night side density does lead to increased reconnection of the IMF to the southern anomalous magnetic field when the SSMA are on the dawn and dusk sides though. The IMF, which is held off the surface by the ionosphere, can penetrate to a lower altitude due to the reduced density, allowing reconnection in regions that the IMF is excluded from for the equal night side density cases. The magnetic field configuration for the night side case is similar in both equal and reduced night side density cases.

[38] The sensitivity of the results to conditions inside the inner boundary was also tested. The anomalous magnetic field is held static in time everywhere in the grid, but the value that it was held static at inside the inner boundary was varied. The resulting plasma asymmetries and magnetic field geometry were virtually identical to above results, including the midnight SSMA case, which has significant modification of the nightside plasma and magnetic field near the surface. This indicates that the formation of the minimagnetopauses and plasma asymmetries is not due to the interaction between the static magnetic field and the time-dependent magnetic field inside the inner boundary.

[39] The resistivity of the inner boundary was also altered to investigate how changes in magnetic reconnection inside the inner boundary, due to reduced diffusion of the IMF through the inner boundary, effect the results outside of the planet. The value of η in equation (6) was also set to 100 ohm m and 0.01 ohm m, with the lower value being comparable to resistivities in the ionosphere. Figure 11 shows the percent change in the pressure and density, and the magnetic fieldlines for the dawn SSMA case when the resistivity of the inner boundary was reduced to 0.01 ohm m and the anomalous magnetic field inside the inner boundary was held static at a nonzero value. The magnetic field geometry changes in both the 100 ohm m and 0.01 ohm m cases, but the general characteristics remain the same. Magnetic fieldlines in the solar wind on the dusk side are connected to the surface on the dawn side, and near the midnight sector, the magnetic field still locally follows lines of constant longitude (L in Figure 11).

[40] In the 100 ohm m case, the percent change in the plasma pressure, temperature and density is nearly identical to when the resistivity is 1000 ohm m. The maximum and minimum change in the density remains the same as in Figure 6, as does the general shape of the asymmetries. When the resistivity of the inner boundary is equal to 0.01 ohm m, the general characteristics of the asymmetries are similar but the tail plasma is not as asymmetric as in Figure 6. Enhancements in the pressure and density are still present near the surface at the dawn terminator, near the SSMA, and the dawn side of the midnight sector (Figures 11a and 11b), but the maximum values are smaller than the high resistivity cases.

[41] When the resistivity is 0.01 ohm m, the tail is more dense in comparison to the case in Figure 6. For example, at approximately 1600 km from the surface on the night side, the density is 50% larger. This is due to the fact that less IMF reaches the surface, and as a result, there is less reconnection of the IMF to the anomalous magnetic field and less plasma impacts the surface. Loss to the surface in Figure 6 is partially driven by the formation of cusp-like structures. The reduction of this loss mechanism, inflates the tail. With the effects of the cusps reduced, the results will resemble the case with no anomalous magnetic field, hence a more symmetric magnetosphere will form.

[42] These features are manifest by a widening of the tail and an increase in the standoff distance of the bow shock. The bow shock form ~600 km further from the surface, at the subsolar point, in the 0.01 ohm m case. No substantial change in the bow shock location occurs for the 100 ohm m

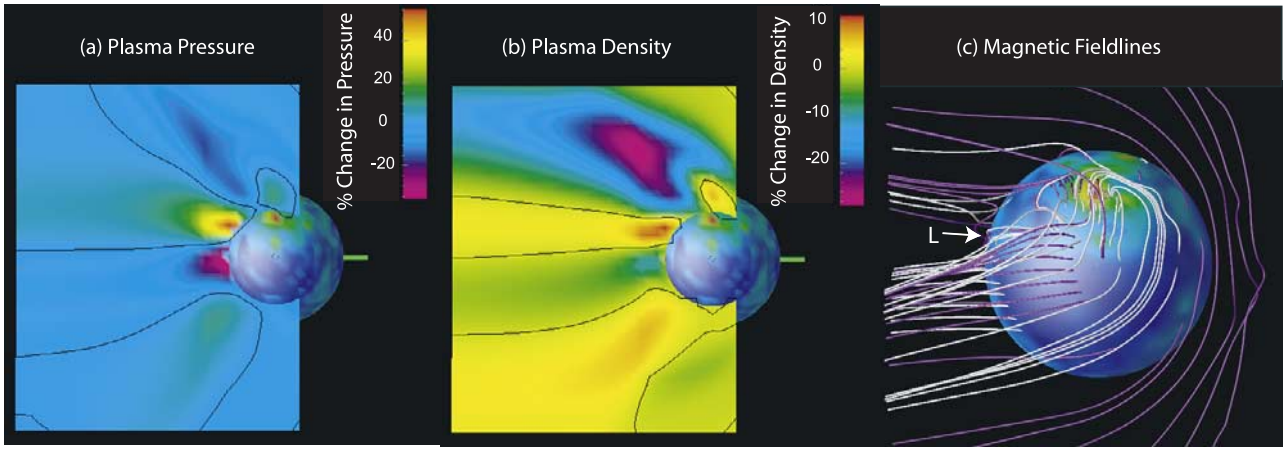

Figure 11. SSMA at the dawn, low resistivity: The percent change in (a) pressure and (b) density, and (c) the magnetic fieldlines for the dawn SSMA case with different boundary conditions. The anomalous magnetic field is static at values different than zero inside the inner boundary and the resistivity of the inner boundary is reduced by five orders of magnitude (to 0.01 ohm m) from the value for the results in Figure 6. All other initial conditions are the same as in Figure 6, and the orientation of the plots is also the same.

case. For the case of a resistivity equal to 100 ohm m, the tail widened by ~450 km, or one grid point, at 3.3 R_M downstream. For the 0.01 ohm m case, the tail widened by ~2800 km, or 40% at 3.3 R_M downstream.

4. Discussion

[43] The simulation results predict that the Martian magnetic anomalies not only modify the plasma locally but can also modify the plasma several Martian radii down the tail. This modification takes the form of asymmetries in the tail plasma density, temperature, pressure, magnetic field, and flow. In addition to modifying the plasma density and temperature, the presence of magnetic anomalies can change the tail width both near the planet and several radii downstream. While the details of the structures that form, particularly the shape and location of minimagnetopauses, are dependent on SSMA orientation and the solar wind conditions, the fact that asymmetric structures form is not dependent on particular SSMA locations or solar wind conditions. Large-scale asymmetries form for a range of anomalous magnetic field orientations.

[44] A minimagnetopause structure forms around or near the SSMA for all three magnetic anomaly orientations investigated. When the strong southern anomalies are located at the dawn or dusk terminator, a minimagnetopause forms just inside the MPB. Previous simulations for the SSMA on the day side that showed the formation of a minimagnetopause in place of the MPB. However, the orientation of the SSMA determines if the anomalous magnetic field also pushes the MPB away from the surface. The simulations show both regions of reconnection of the anomalous magnetic field to the IMF and protected regions. This lends insight into how an intrinsic magnetic field could both locally increase the scale height of the ionosphere (as suggested by *Shinagawa and Cravens* [1989, 1992] and *Axford* [1991]), as well as accelerate ions (as suggested by *Axford* [1991]).

[45] The regions of low plasma pressure and density surrounded by regions of high density and pressure are reminiscent of the flux spikes and plasma voids in MGS electron data [*Mitchell et al.*, 2001]. A satellite traveling through the low pressure and density regions would measure a decrease in electron flux while the magnetic field magnitude increases. The decrease of plasma in the simulation plasma voids is not nearly as strong as that shown by *Mitchell et al.* [2001], where the electron flux decreases by nearly two orders of magnitude from the nominal flux nearby. None of the plasma voids in the simulation results show a decrease in density of even an order of magnitude when compared to either the nearby plasma density or the tail density when no anomalies are present. The scale size of both the measured and model plasma voids are comparable though, being on the order of 1000 km. In addition, the closed magnetic field lines in the plasma voids measured by MGS are seen at the simulation plasma voids as well.

[46] The flux spikes seen by *Mitchell et al.* [2001] between successive plasma voids had an energy spectrum similar to magnetosheath plasma. This and the radial magnetic field geometry indicated that the magnetic field lines were once connected to the IMF. If the ions in this region were also of magnetosheath origin, it suggests the plasma in the flux spike region would be hotter than ionospheric plasma. While radial magnetic fields are prevalent in the simulation results, the only temperature enhancements are seen where a minimagnetopause forms and even then the temperature is comparable to the surface ionospheric temperature and at least an order of magnitude smaller than the temperature of the sheath plasma. The flux spikes may be dynamic features, that are not seen in the simulation due to the fact that the planet is not rotated during a simulation run and, maybe more importantly, the solar wind conditions are held steady. An ionosphere modeled with light ions that are not gravitationally bound, may also result in preventing access to the surface by magnetosheath plasma.

[47] When *Kar et al.* [1996] calculated the diffusive equilibrium profile expected for O_2^+ density, they found that their model predicted higher densities above 150 km than

measured by the Viking landers. Their estimated outflow rate was also an order of magnitude smaller than measured by Phobos2 [*Lundin et al.*, 1990]. This suggested to Kar et al. that there is a "missing component" governing the ionospheric outflow rates at Mars. This missing component may be the magnetic anomalies and their interaction with the IMF. As the results in this paper show, the presence of the anomalous magnetic field not only changes the plasma flow near the surface, but that change is also dependent on the location of the strongest magnetic anomalies relative to the IMF orientation.

[48] The next step in the simulations will be to extend the model to account for multiple ion species by including heavy ion dynamics. Besides having negligible gravitational effects due to the uniform mass, the single fluid model presented here cannot determine absolutely which population, the ionosphere or the solar wind, is primarily responsible for the asymmetries in the plasma densities. It can only be inferred in the single fluid model that the asymmetries are due to ionospheric plasma since the temperature of the plasma in the tail region, even near the asymmetries, is cold compared to the magnetosheath plasma. The results also can say nothing about any mass dependence in the asymmetric regions. The ability to track separate populations, with mass differences, in the multifluid treatment will help resolve the effects of the magnetic anomalies on the ionospheric outflow rates by separating ionospheric populations from the solar wind, as well as investigating how the anomalous magnetic field controls the dynamics of the ionospheric outflows. Including the ion-cyclotron effects, that are part of the multifluid approach [*Winglee*, 2004], will also capture ion-cyclotron induced asymmetries such as the asymmetric bow shock that is seen in the data and is currently only captured by hybrid models of an unmagnetized Mars [cf. *Brecht*, 1997; *Kallio and Janhunen*, 2002].

[49] Also needed are simulations with variable solar wind conditions. The results presented here show only one IMF configuration to highlight asymmetries caused by changes in the anomalies magnetic field orientation. Dynamic changes in the IMF strength and orientation may lead to transient asymmetries generated by reconnection events similar to those that occur in the Earth's tail during changes between northward and southward IMF, and which may be responsible for some of the asymmetric heavy ion flows measured by satellites [cf. *Lundin et al.*, 1990].

[50] **Acknowledgments.** The authors would like to thank J. C. Cain for providing the source code to generate the model Martian magnetic field. This research was supported by a NASA Graduate Student Research Fellowship, NASA grant NAG 5-11869, and NSF grant ATM-0105032.

[51] Arthur Richmond thanks the reviewers for their assistance in evaluating this manuscript.

References

Acuna, M. H., et al. (1999), Global Distribution of Crustal Magnetization Discovered by the Mars Global Surveyor MAG/ER Experiment, *Science*, *284*, 790–793.

Axford, W. I. (1991), A commentary on our present understanding of the Martian magnetosphere, *Planet. Space Sci.*, *39*, 167–173.

Brace, L. H., and A. J. Kliore (1991), The structure of the Venus ionosphere, *Space Sci. Rev.*, *55*, 81–163.

Brecht, S. (1997), Hybrid simulations of the magnetic topology of Mars, *J. Geophys. Res.*, *102*, 4743–4750.

Dubinin, E., et al. (1991), Comparison of observed plasma and magnetic field structures in the wakes of Mars and Venus, *J. Geophys. Res.*, *96*, 11,189–11,197.

Cain, J. C., B. B. Ferguson, and D. Mozzoni (2003), An $n = 90$ internal potential function of the Martian crustal magnetic field, *J. Geophys. Res.*, *108*(E2), 5008, doi:10.1029/2000JE001487.

Connerney, J. E. P., et al. (1999), Magnetic lineations in the ancient crust of Mars, *Science*, *284*, 794–798.

Crider, D. H., et al. (2000), Evidence of electron impact ionization in the magnetic pileup boundary of Mars, *Geophys. Res. Lett.*, *27*, 45–48.

Crider, D. H., et al. (2002), Observations of the latitude dependence of the location of the martian magnetic pileup boundary, *Geophys. Res. Lett.*, *29*(8), 1170, doi:10.1029/2001GL013860.

Hanson, W. B., et al. (1977), The Martian ionosphere as observed by the Viking retarding potential analyzers, *J. Geophys. Res.*, *82*, 4351–4363.

Harnett, E. M., and R. M. Winglee (2003), The influence of a mini-magnetopause on the magnetic pileup boundary at Mars, *Geophys. Res. Lett.*, *30*(20), 2074, doi:10.1029/2003GL017852.

Kallio, E., and P. Janhunen (2002), Ion escape from Mars in a quasi-neutral hybrid model, *J. Geophys. Res.*, *107*(A3), 1035, doi:10.1029/2001JA000090.

Kallio, E., et al. (1995), Oxygen outflow in the Martian magnetotail, *Geophys. Res. Lett.*, *22*, 2449–2453.

Kar, J., et al. (1996), On the outflow of O_2^+ ions at Mars, *J. Geophys. Res.*, *101*, 12,747–12,752.

Lundin, R., et al. (1989), First measurements of the ionospheric plasma escape from Mars, *Nature*, *341*, 609–612.

Lundin, R., et al. (1990), ASPERA/PHOBOS measurements of the ion outflow from the Martian ionosphere, *Geophys. Res. Lett.*, *17*, 873–876.

Ma, Y., A. F. Nagy, K. C. Hansen, D. L. DeZeeuw, T. I. Gombosi, and K. G. Powell (2002), Three-dimensional multispecies MHD studies of the solar wind interaction with Mars in the presence of crustal fields, *J. Geophys. Res.*, *107*(A10), 1282, doi:10.1029/2002JA009293.

Mitchell, D. L., et al. (2001), Probing Mars' crustal magnetic field and ionosphere with the MGS Electron Reflectometer, *J. Geophys. Res.*, *106*, 23,419–23,427.

Riedler, W., et al. (1989), Magnetic field near Mars, *Nature*, *341*, 604–607.

Richtyer, R. D., and K. W. Morton (1967), *Difference Methods for Initial-Value Problems*, Wiley Interscience, Hoboken, N. J.

Rosenbauer, H., et al. (1989), Ions of Martian origin and plasma sheet in the Martian magnetosphere: Initial results from the TAUS experiment, *Nature*, *341*, 612–614.

Shinagawa, H., and T. E. Cravens (1989), A one-dimensional multispecies magnetohydrodynamic model of the dayside ionosphere of Mars, *J. Geophys. Res.*, *94*, 6506–6516.

Shinagawa, H., and T. E. Cravens (1992), The ionospheric effects of a weak intrinsic magnetic field at Mars, *J. Geophys. Res.*, *97*, 1027–1035.

Tang, C. H., et al. (1977), Bistatic radar measurements of the electrical properties of the Martian surface, *J. Geophys. Res.*, *82*, 4305–4315.

Verigin, M. I., et al. (2001), Evidence of the influence of equatorial Martian crustal magnetization on the position of the planetary magnetotail boundary by Phobos 2 data, *Adv. Space Res.*, *28*, 885–889.

Vignes, D., et al. (2000), The solar wind interaction with Mars: locations and shapes for the bow shock and the magnetic pile-up boundary from the observations of the MAG/ER experiment onboard Mars Global Surveyor, *Geophys. Res. Lett.*, *27*, 49–52.

Winglee, R. M. (2004), Ion cyclotron and heavy ion effects on reconnection in a global magnetotail, *J. Geophys. Res.*, *109*, A09206, doi:10.1029/2004JA010385.

E. M. Harnett and R. M. Winglee, Department of Earth and Space Sciences, Box 351310, University of Washington, Seattle, WA 98195-1310, USA. (eharnett@ess.washington.edu; winglee@ess.washington.edu)